

Mach-Zehnder interferometry method for acoustic shock wave measurements in air and broadband calibration of microphones

Petr Yuldashev,^{a),b)} Maria Karzova,^{b)} and Vera Khokhlova^{c)}

Faculty of Physics, M.V. Lomonosov Moscow State University, Moscow 119991, Russia

Sébastien Ollivier

Laboratoire de Mécanique des Fluides et d'Acoustique, Unité Mixte de Recherche, Centre National de la Recherche Scientifique 5509, École Centrale de Lyon, Université Lyon 1, 36 Avenue Guy de Collongue, 69131 Écully Cedex, France

Philippe Blanc-Benon

Laboratoire de Mécanique des Fluides et d'Acoustique, Unité Mixte de Recherche, Centre National de la Recherche Scientifique 5509, École Centrale de Lyon, Université Lyon, 36 Avenue Guy de Collongue, 69131 Écully Cedex, France

(Received 24 July 2014; revised 30 April 2015; accepted 8 May 2015)

A Mach-Zehnder interferometer is used to measure spherically diverging N -waves in homogeneous air. An electrical spark source is used to generate high-amplitude (1800 Pa at 15 cm from the source) and short duration (50 μ s) N -waves. Pressure waveforms are reconstructed from optical phase signals using an Abel-type inversion. It is shown that the interferometric method allows one to reach 0.4 μ s of time resolution, which is 6 times better than the time resolution of a 1/8-in. condenser microphone (2.5 μ s). Numerical modeling is used to validate the waveform reconstruction method. The waveform reconstruction method provides an error of less than 2% with respect to amplitude in the given experimental conditions. Optical measurement is used as a reference to calibrate a 1/8-in. condenser microphone. The frequency response function of the microphone is obtained by comparing the spectra of the waveforms resulting from optical and acoustical measurements. The optically measured pressure waveforms filtered with the microphone frequency response are in good agreement with the microphone output voltage. Therefore, an optical measurement method based on the Mach-Zehnder interferometer is a reliable tool to accurately characterize evolution of weak shock waves in air and to calibrate broadband acoustical microphones. © 2015 Acoustical Society of America.

[<http://dx.doi.org/10.1121/1.4921549>]

[MDV]

Pages: 3314–3324

I. INTRODUCTION

Accurate measurements of broadband acoustic signals in air, particularly high-amplitude shock N -waves generated by explosion-type sources or small supersonic projectiles, remain a challenge. The need for such measurements arises, for example, in problems concerning acoustical emission from small charge explosions or gunshots.^{1–7} Also, spark generated N -waves are used to sonify downscaled models in architectural, hall, and street acoustics^{8,9} or in laboratory-scale experimental studies of the propagation of sonic booms in the atmosphere.^{10–12}

The bandwidth of commercially available high-frequency condenser microphones does not typically exceed 150 kHz (at –3 dB level), while the spectrum of acoustic pulses with shocks extends beyond 1 MHz.⁵ The limited bandwidth and resonances of frequency response of such microphones result

in significant distortions of the measured waveforms and in the over-estimation of shock rise times.¹³ Piezoresistive and piezoelectric dynamic pressure sensors have extended bandwidth, but also have a lower sensitivity (14.5 mV/kPa for the model 113B28 PCB Piezotronics). Manufacturers of commercial microphones usually provide incomplete information about frequency response: it is measured over a limited range of frequencies and only the magnitude of the response (without phase) is given.^{14,15} Also it is known that frequency response depends on microphone mounting and housing type.^{5,16} It has been shown that better results are obtained when the microphone is mounted in a rigid baffle which is used to postpone diffracted waves. However, even in this case the response depends on fine adjustment of the microphone in the baffle. Currently, new types of microphones fabricated using microelectromechanical systems technologies with potentially up to 1 MHz bandwidth are being proposed.^{17–19} Thus, development of calibration methods for broadband microphones and evaluation of their frequency response is a relevant problem of experimental aeroacoustics.^{5,20}

Optical methods provide alternative possibilities to measure acoustic waves. The numerous existing methods can be classified according to shadowgraphy, schlieren, and interferometry families.^{21,22} The shadowgraphy methods are

^{a)}Electronic mail: petr@acs366.phys.msu.ru

^{b)}Also at: Laboratoire de Mécanique des Fluides et d'Acoustique, Unité Mixte de Recherche, Centre National de la Recherche Scientifique 5509, École Centrale de Lyon, Université Lyon, 36 Avenue Guy de Collongue, 69131 Écully Cedex, France.

^{c)}Also at: Center for Industrial and Medical Ultrasound, Applied Physics Laboratory, University of Washington, 1013 NE 40th Street, Seattle, WA 98105, USA.

mainly sensitive to sharp changes of pressure, i.e., shocks, but smooth variations of pressure in the acoustic wave are missed.¹³ Schlieren methods are more sensitive and a whole waveform can be measured. The best sensitivity is provided by interferometer-based methods.²³ Recently it has been shown that a laser Doppler vibrometer (LDV) can be used to measure spatial pressure distribution of acoustic waves.^{24,25} An LDV can provide bandwidth up to several tens of MHz which is appropriate for measurements of shock waves produced by a spark. However, we propose a cheaper solution using a Mach-Zehnder interferometer, which has similar performance. Many implementations of optical microphones are listed in the review of Bilaniuk.²⁶ However, none of the presented examples are suitable for measurements of broadband shock waves due to bandwidth limitations.

In this work an alternative optical method for measurement of spherical acoustic pulses is theoretically analyzed and the experimental setup is realized. The design of the optical part of the experimental setup was based on the work of Smeets who used a Mach-Zehnder interferometer as a high-frequency microphone.²⁷ In his experiment only a small part (10 mm) of a probing laser beam of the interferometer was exposed to acoustic waves. All other optical paths along the probing and reference beams were covered by protecting tubes. Such a design implies that artificial reflections from the edges of the protecting tubes contaminate the measured signal. In his paper Smeets showed that phase signals corresponding to *N*-wave and unwanted reflections are clearly seen (Fig. 5 of Ref. 27). The difference with Smeets' experiment is that a whole propagation path of the probing laser beam was established to interact with the acoustic wave. Thus, any artificial perturbations of a measured signal corresponding to a direct wave were avoided. The most important achievement of the current study is that, assuming spherical wave propagation in homogeneous air, a waveform reconstruction method based on an Abel-type inversion algorithm is proposed and validated. The frequency bandwidth of the optical method is estimated to be in range of 2.5 MHz which is 6 times better than the bandwidth of 1/8-in. condenser microphones (Brüel & Kjær, B&K¹⁵ and G.R.A.S., Denmark¹⁴).

Accurate measurements provided by the interferometric method allowed the development of a procedure for calibrating standard acoustic microphones. A condenser microphone (B&K, type 4138) was placed 51.2 mm behind the probing laser beam to record the same acoustic pulse propagating first through the laser beam and then with some delay arriving to the microphone. Waveform modification along this 51.2 mm propagation path due to different propagation effects (nonlinearity, thermoviscous absorption, and molecular relaxation) was taken into account using a generalized Burgers equation.^{20,28} The frequency response of the microphone (amplitude and phase) was obtained by comparing the spectra of the waveforms resulting from optical and acoustical measurements. It is shown that the optically measured waveforms filtered with the microphone frequency response are in good agreement with the waveforms recorded by the microphone at different available propagation distances.

This paper is organized as follows. The experimental setup and the waveform reconstruction method are detailed

in Sec. II. Then the results of optical measurements are given and compared with a theoretical propagation model in Sec. III. A calibration method for condenser microphones is presented in Sec. IV. Results are summarized in Sec. V.

II. EXPERIMENTAL METHOD

A. Experimental setup

1. Spark source and condenser microphone

The experimental setup includes optical and acoustical parts (Fig. 1). In the acoustic part an electrical spark source is used to generate short duration and high pressure acoustic pulses often called as *N*-waves due to their specific waveform.^{1,5} The spark source is made of two tungsten electrodes, separated by a gap of 20 mm, and supplied by a high voltage electrical source (16–20 kV). Condensers are connected in parallel with electrodes in order to accumulate electrical charge. The voltage between the electrodes increases until the potential of air breakdown is reached, and then a spark is generated. The sudden local heating produces a high amplitude and short duration pressure pulse. During measurements the spark source was running in permanent mode generating the acoustic pulses with a repetition rate of about 1 Hz.

Acoustical measurements were performed using a broadband microphone (B&K, type 4138 1/8-in. microphone) coupled with an adapted preamplifier (B&K 2670) and amplifier (B&K Nexus amplifier with extended bandwidth: –3 dB at 200 kHz). The microphone without its protection grid was mounted in a baffle in order to minimize diffraction effects on its edge. The recorded signals were digitized (12 bit, 10 MHz) using a data acquisition card (National Instruments PXI-1033). The microphone was placed 51.2 mm behind the probing laser beam of the interferometer in front of the spark source (Fig. 1) in order to

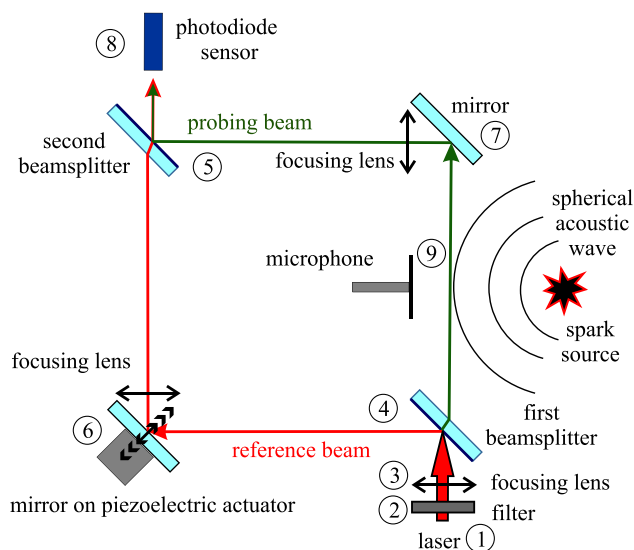


FIG. 1. (Color online) Illustration of the experimental setup (top view). Spark-generated *N*-wave propagates through the probing laser beam of the Mach-Zehnder interferometer altering the optical phase difference relative to the reference beam. An acoustical microphone is placed behind the probing beam to provide simultaneous measurements of the waveform by acoustical and optical methods.

provide sufficient delay for the wave reflected from the baffle and traveling back in the direction of the probing beam. In this way, contamination of the optical measurement of the primary wave is avoided.

2. Mach-Zehnder interferometer

The Mach-Zehnder interferometer was mounted on a 60×60 cm optical breadboard (PBH51505, ThorLabs, Inc.) and was composed of a laser source ①, two beam splitters (④ and ⑤, 50/50 reflection/transmission), two flat mirrors ⑥ and ⑦, three lenses ③, and a photodiode sensor ⑧ (Fig. 1). A He-Ne laser (wavelength $\lambda = 632.8$ nm) with a nominal power of 10 mW was used as a coherent light source. Neutral filters were used to attenuate the light beam power down to 1.3 mW to fit requirements of the photodiode sensor ②. All optical elements (beamsplitters, mirrors, filters, and lenses) were 25 mm in diameter. The first beamsplitter ④ divides the incident laser beam into a *reference beam* and a *probing beam*. The second beamsplitter sums these two beams to produce an interference intensity pattern at the photodiode surface. The beamsplitters only approximately fitted the declared 50/50 reflection and transmission coefficients. However, in the chosen propagation scheme the probing beam is first transmitted and then reflected while the reference beam is reflected and then transmitted. Thus, deviation of reflection and transmission coefficients from 50/50 ratio is compensated and beams had almost equal intensities at the exit. Propagation paths of the reference and the probing beams formed a square with 35 cm side.

A focusing lens with 20 cm focal length was mounted between the laser and the first beam splitter in order to reduce the probing beam thickness in the zone where the interaction with the acoustic wave occurs ⑨. Thinner probing beam provides better time resolution of the measurement method. Two other focusing lenses (15 cm focal length) were placed a few centimeters after each of the two mirrors. These lenses compensate the divergence of the laser beam and reduce the beam cross-section in order to collect its total optical power on the surface of the photodiode. The beams were aligned in such a way that the output optical field contained only one interferometric fringe. Thus, functioning of the interferometer in the infinite-fringe mode was realized.²²

Light intensity at the exit of the interferometer was captured by a photodiode (NT53–372, Edmund Optics) which has responsivity $r_p = 0.35$ A/W at 632.8 nm optical wavelength, a surface of 3.2 mm^2 , and 45 pF of electric capacitance at zero bias voltage. The photodiode was connected to a transimpedance amplifier to provide a linear relation between the light intensity and the output voltage. The transimpedance amplifier was designed according to the guidelines given in Fig. 3.14 of Ref. 29. The transmission impedance of the amplifier was $R = 2.2 \text{ k}\Omega$. Thus, the output voltage u_{ph} of the photodiode amplifier is related to the beam power P as $u_{ph} = r_p R P$. A low noise constant reverse bias (2.5 V) was applied to the photodiode to reduce its capacitance and to increase the bandwidth of the amplifier up to 16 MHz (at -3 dB).

The output voltage of the photodiode amplifier u_{ph} was fed to the first input of a fully differential amplifier with unit gain and 26 MHz bandwidth. An adjustable low noise

reference voltage source was connected to the second input of the differential amplifier to provide necessary bias to the resulting output signal. The optical signal was measured at the first output of the differential amplifier. Inverted signal from the second output of the differential amplifier (u_{fb}) was applied to an input of the feedback loop of a stabilization system.

In the stabilization system the input voltage u_{fb} was filtered by a first-order low-pass filter with $\tau_f = 20$ ms time constant. The output of the filter was connected to a low-frequency amplifier (25 kHz bandwidth, gain 10) which was loaded to a piezoactuator. One mirror was glued to the piezoactuator; thus its small displacement provided control on the optical phase difference between the reference and the probing beams (Fig. 1, ⑥). The piezoactuator (AE0505D08F, ThorLabs) lengthening coefficient was equal to $\varkappa = 9.1 \times 10^{-8}$ m/V. The piezoactuator produces the optical phase shift, which is proportional to the applied voltage u_{pz} ,

$$\varphi_{pz}(t) = 2\sqrt{2}k_0\varkappa u_{pz}(t) = \alpha u_{pz}(t), \quad (1)$$

where $k_0 = 2\pi/\lambda$ is the optical wavenumber. The numeric coefficient $2\sqrt{2}$ in Eq. (1) appears due to the fact that the piezoactuator moves the mirror along a diagonal between the incident and the reflected light beams forming a right angle (Fig. 1). The parameter $\alpha = 2\sqrt{2}k_0\varkappa$ in the given experimental conditions was equal to 2.56 V^{-1} .

B. Optical signal formation

Light intensity I formed by the interference of the reference and the probing beams at the surface of the photodiode is described by the following equation:³⁰

$$I = I_A + I_B + 2\sqrt{I_A I_B} \cos(\varphi), \quad (2)$$

where I_A and I_B are the intensities of the probing and the reference beams after the second beamsplitter, respectively, and φ is the optical phase difference between them. The measurement protocol was organized as follows. At the first stage, the laser source was disabled and the input bias to the differential amplifier was adjusted in the way to produce zero output signal. Thus, light intensity I is proportional to the output voltage signal and the same equation is applied,

$$u_D = u_A + u_B + 2\sqrt{u_A u_B} \cos(\varphi). \quad (3)$$

Here, u_A is the voltage measured when the reference beam is shaded, and u_B when the probing beam is shaded. Excitation of low-frequency mechanical oscillations of the experimental setup produced corresponding variations of the optical phase difference. These low-frequency phase variations were used to check the quality of the interference. It was verified that the minimal value of the measured voltage is equal to $u_{Dmin} = u_A + u_B - 2\sqrt{u_A u_B}$, and the maximal value is equal to $u_{Dmax} = u_A + u_B + 2\sqrt{u_A u_B}$. At the second stage, the bias voltage was moved to the position where the output voltage is equal to $u_C = -(u_A + u_B)$ in the absence of the optical signal from the photodiode. In this case, when the optical signal is turned on, the output voltage of the differential amplifier is proportional to the cosine function of the phase argument φ ,

$$u = u_D + u_C = 2\sqrt{u_A u_B} \cos(\varphi) = u_0 \cos(\varphi), \quad (4)$$

where $u_0 = 2\sqrt{u_A u_B}$ is the amplitude of voltage variations.

The total phase difference φ is the sum of the following items:

$$\varphi(t) = \varphi_0 + \varphi_{pz}(t) + \varphi_{ac}(t) + \varphi_n(t). \quad (5)$$

Here φ_0 is a constant phase difference related to initial adjustment of the interferometer, $\varphi_{ac}(t)$ is a phase difference produced by the measured acoustic wave, and $\varphi_n(t)$ is a phase related to mechanical perturbations: ground vibrations, acoustic noise, air flows. For example, the interferometer was sensitive even to voice and clapping hands.

The stabilization system was designed to keep the output voltage at zero level in the absence of acoustic waves by compensating low-frequency noise and forcing the phase φ to remain close to the $\pi/2$ value. The functioning of the system is described in the Appendix. As a result, the output voltage is related to the phase difference associated with the measured acoustic wave as

$$u = u_0 \sin(\varphi_{ac}(t) + \varphi_r(t)), \quad (6)$$

where $\varphi_r(t)$ is a fraction of the noise that was not completely compensated by the stabilization system. Some uncompensated constant offsets also could be present in the function $\varphi_r(t)$. However, as the spectrum of the acoustic phase $\varphi_{ac}(t)$ is concentrated at high frequencies above several kHz and the noise phase $\varphi_r(t)$ is generally a low-frequency function (from 0 to 100 Hz), it was always possible to subtract this component, which appeared as an almost constant bias during the acquisition time window.

C. Optical phase induced by the acoustic wave

In the acoustic wave perturbations of pressure p , density ρ and optical refraction index n are related one to another. Pressure and density are related as³¹

$$p + p_0 = p_0(1 + \rho/\rho_0)^\gamma, \quad (7)$$

where γ is the specific heat ratio, and p_0 and ρ_0 are ambient pressure and density, respectively. The linearization of Eq. (7) gives

$$p = \rho c_0^2, \quad (8)$$

where $c_0 = \sqrt{\gamma p_0/\rho_0}$ is the speed of sound. The optical refraction index perturbation is proportional to the density perturbation,

$$n = G\rho, \quad (9)$$

where $G = 0.000226 \text{ m}^3/\text{kg}$ is the Gladstone-Dale constant at 632.8 nm wavelength.²²

A radially symmetric acoustic wave traveling through the probing beam is schematically drawn in Fig. 2. The probing beam is located at the distance $x = r_1$ from the spark

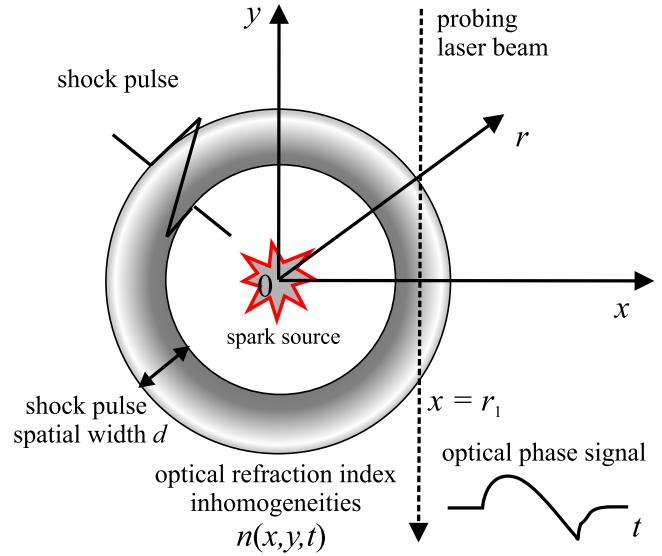


FIG. 2. (Color online) Illustration of the optical phase integration along the probing laser beam propagating through a radial distribution of the refraction index inhomogeneities induced by the acoustic wave.

source. At any time t , the refraction index distribution $n(x, y, t)$ induced by the acoustic wave leads to a phase difference,

$$\varphi_{ac}(t) = k_0 \int_{-\infty}^{+\infty} n(x = r_1, y, t) dy. \quad (10)$$

Since the distribution $n(x, y, t) = n(r, t)$ is a radially symmetric function, Eq. (10) can be written as

$$\varphi_{ac}(t) = 2k_0 \int_{r_1}^{+\infty} \frac{n(r, t) r dr}{\sqrt{r^2 - r_1^2}}. \quad (11)$$

The analytical inversion of Eq. (11) to obtain $n(r, t)$ is not known. However, as functions $n(r, t)$ at different times t are not independent and belong to the same traveling acoustic wave, an approximate method to reconstruct the function $n(r = r_1, t)$ from the phase signal $\varphi_{ac}(t)$ is proposed and described in Sec. IID.

Note also, that the integration along the straight line $x = r_1$ in Eqs. (10) and (11) implies that the finite widths of the laser beam and diffraction effects, which change the structure of the beam, are not taken into account. In order to check that neglecting the finite beam width and diffraction effects do not alter the accuracy of the method, these effects were analyzed using numerical simulations of the optical field propagation through inhomogeneities of refraction index produced by the acoustic wave.³² For typical experimental conditions (peak pressure 1000 Pa, shock rise time $0.15 \mu\text{s}$, beam width 0.1–0.5 mm) it has been shown that the time resolution of the method is mainly determined by the finite beam width (0.2 – $0.4 \mu\text{s}$) and diffraction effects do not lead to perturbation of the optical beam structure.

The sensitivity of the optical phase to the acoustic pressure $S_{a\varphi} = \varphi_{ac}/p$ depends on the radius of the wavefront at the point where the acoustic wave is crossing the beam (here

it is r_1). If the width of the acoustic pulse is denoted as d (Fig. 2), then the integration path along the laser beam in Eq. (10) is estimated to be $L \approx 2\sqrt{2r_1d}$ and it is proportional to $\sqrt{r_1}$. According to Eqs. (8) and (9) the acoustic phase is on the order of

$$\varphi_{ac} \approx k_0GL \frac{P}{c_0^2} \approx k_0G2\sqrt{2r_1d} \frac{P}{c_0^2}. \quad (12)$$

In the given experimental conditions, $d \approx 1$ cm, $c_0 \approx 340$ m/s, the pressure is of order of 1000 Pa at $r_1 = 20$ cm from the spark source.²⁰ Thus, the optical phase is about 2.5 radians. Even at a distance $r_1 = 1.0$ m, where the pressure amplitude is attenuated down to 150 Pa, the phase is about 0.8 radians, which is nevertheless sufficient to be detected.

D. Optical signal processing

The two previous sections described what happens when an acoustic wave crosses a laser beam and how the optical phase difference is formed. In the current section the optical signal processing and the pressure waveform reconstruction method are described.

In the signal processing sequence the high frequency electrical noise was filtered, taking care to preserve the shock front by using time windows. The phase signal was obtained according to Eq. (6)

$$\varphi_{ac}(t) + \varphi_r(t) = \arcsin(u/u_0). \quad (13)$$

Then the low-frequency noise $\varphi_r(t)$, which appears as a background constant, was removed.

The main difficulty in the waveform reconstruction method is to find the function $n(r = r_1, t)$ if the function $\varphi_{ac}(t)$ in the integral Eq. (11) is known. Equation (11) in its form is similar to the well known Abel transform,³³

$$A(r) = \int_r^{+\infty} \frac{2f(r')r'dr'}{\sqrt{r'^2 - r^2}}, \quad (14)$$

whose inverse is given by

$$f(r) = -\frac{1}{\pi} \int_r^{+\infty} \frac{\partial A(r')}{\partial r'} \frac{dr'}{\sqrt{r'^2 - r^2}}. \quad (15)$$

The Abel transform and its inverse operate on stationary functions of a radial distance r . On the contrary, in Eq. (11) two variables, radial distance and time, are involved and the function $n(r, t)$ can be regarded as a moving object which is changing due to acoustic propagation. As the signal $\varphi_{ac}(t)$ is obtained only at the fixed radial distance $r = r_1$, the reconstruction of the function $n(r = r_1, t)$ is approximative.

The reconstruction algorithm is based on the inverse Abel transform. Since the acoustic wave does not change too much over a propagation distance equal to its wavelength (for the N -wave it is the distance between front and rear shocks), the moving object $n(r, t)$ can be treated as a stationary function at some fixed time t , while the laser beam is supposed to move along the x axis with the sound speed c_0 . The algorithm consists of three steps.

- (1) Using the coordinate transform $t = t_s - (r - r_1)/c_0$, the phase signal $\varphi_{ac}(t)$ is written as a function of the radial distance r : $\varphi_{ac}(t_s - (r - r_1)/c_0) = \tilde{\varphi}_{ac}(r)$. Here, t_s is a time shift constant which determines which part of the signal appears at $r = r_1$. For example, t_s can be chosen to fix the front shock position at r_1 .
- (2) Apply the Abel inversion transform (15) to the function $\tilde{\varphi}_{ac}(r)$ resulting in a function $k_0\tilde{n}(r)$.
- (3) Return back to functions of time using inverse coordinate transform $r = r_1 - (t - t_s)c_0$: $\tilde{n}(r) = \tilde{n}(r_1 - (t - t_s)c_0) = n^*(t)$.

The resulting function $n^*(t)$ is an approximate solution for the unknown function $n(r = r_1, t)$. Finally, density and acoustic pressure functions are calculated from $n^*(t)$ using Eqs. (9) and (7). Note that in the approximated reconstruction algorithm, evolution of the waveform due to acoustical propagation effects (nonlinearity, absorption, and relaxation) is neglected. Thus, an additional error is introduced. The mathematical proof of the reconstruction algorithm was beyond the scope of the article, but its performance and accuracy were checked in synthetic tests which are described in Sec. III E.

E. Validation of waveform reconstruction method

In the synthetic tests the calculation steps described in the two previous sections were done numerically for acoustic pulses propagating in typical experimental conditions. Propagation of nonlinear acoustic waves was simulated using the generalized Burgers equation,²⁸

$$\frac{\partial p}{\partial r} + \frac{p}{r} = \frac{\beta}{\rho_0 c_0^3} p \frac{\partial p}{\partial \tau} + \frac{b}{2\rho_0 c_0^3} \frac{\partial^2 p}{\partial \tau^2} + \sum_{\nu=1}^{\nu=2} d_\nu \frac{\partial}{\partial \tau} \int_{-\infty}^{\tau} \exp\left(-\frac{\tau - \tau'}{\tau_\nu}\right) \frac{\partial p}{\partial \tau'} d\tau'. \quad (16)$$

Here, $\tau = t - (r - r_0)/c_0$ is the retarded time, c_0 is the ambient sound speed at low frequencies, $\beta = (\gamma + 1)/2$ is the coefficient of nonlinearity, and b is the coefficient of viscosity in the air. Each relaxation process ν is characterized by two parameters: relaxation time τ_ν and coefficient $d_\nu = (c_\nu^2 - c_0^2)/c_0^2 = c_\nu/c_0^2$, where c_ν^2 is the so-called frozen sound speed of an acoustic signal propagation through the medium with relaxation time much longer than the effective duration of the signal $T_s \ll \tau_\nu$. A numerical algorithm which solves Eq. (16) is described in previous publications of the authors.^{13,20} Acoustic properties of the propagation medium were calculated from thermodynamic properties of dry air that were taken from Ref. 34 and using the moist air model from Ref. 35. Measured values of the ambient pressure, temperature, and relative humidity were used as input parameters for the air model.

Two typical waveforms were chosen to perform the tests: an ideal N -wave^{1,5} (symmetric waveform: the positive peak pressure is equal to the negative peak pressure, Fig. 3, on the right) and a so-called *blast wave*⁷ (nonsymmetric waveform, the negative peak pressure is several times lower than the positive peak pressure, Fig. 3, on the left). The blast

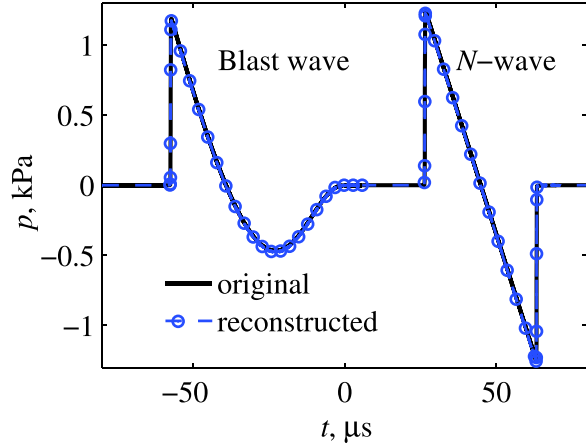


FIG. 3. (Color online) Comparison of reconstructed (dashed line with markers) and original (solid line) waveforms at the distance $r_1 = 20$ cm from the spark source for the cases of an ideal N -wave and a blast wave.

wave fits experimentally measured waveforms better close to the source while at large distances the N -wave is better. Initial waveforms at $r_0 = 10$ cm are set with a 3000 Pa positive peak pressure and a $15 \mu\text{s}$ compression phase duration. The atmospheric conditions were taken to be $p_0 = 100$ kPa, temperature 20°C , and 50% humidity.

The Burgers equation (16) is written with the retarded time τ , thus in the numerical solution at each distance r a waveform $p(r, \tau)$ as a function of τ is given. To perform synthetic tests these waveforms were interpolated to r and t coordinates, i.e., at each time t a spatial waveform $\tilde{p}(r, t) = p(r, t - r/c_0)$ is given. Using Eqs. (7), (9), and (11), the optical phase signal $\varphi_{ac}(t)$ at $r = r_1$ was simulated. Then the function $\varphi_{ac}(t)$ was used as an input function for the reconstruction algorithm, and the approximate solution $n^*(t)$ and corresponding pressure waveform $p^*(t)$ were obtained. The reconstructed waveform $p^*(t)$ was compared with an original waveform $p(r = r_1, t)$ to estimate the accuracy of the algorithm. The comparison is shown in Fig. 3 for a distance of $r_1 = 20$ cm. It is seen that the reconstructed waveforms (dashed lines) only differ slightly from the original ones (solid lines). The reconstruction errors are listed in Table I (N -wave) and Table II (blast wave) for several distances r_1 from 10 to 100 cm. Positive and negative peak pressures (p_+ and p_-), the arrival time t_{ar} and the compression phase duration T of the pulse were considered. It is seen that the amplitude error is of order of 1%–2% or less and decreases at larger distances r . It was also checked that varying the time shift constant t_s in a range corresponding to the duration of the acoustic pulse, the reconstructed waveforms did not

TABLE I. Accuracy of the reconstruction algorithm for an ideal N -wave at different distances from the spark source.

r_1 (cm)	10	15	20	40	60	100
$\Delta p_+/p_+$ (%)	2	1.6	1.3	0.7	0.5	0.4
$\Delta p_-/p_-$ (%)	0.5	0.9	0.7	0.5	0.5	0.2
$\Delta T/T$ (%)	0.6	0.5	0.3	0.5	0.2	0.4
Δt_{ar} (μs)	0.03	0.03	0.03	0.03	0.03	0.03

TABLE II. Accuracy of the reconstruction algorithm for a blast wave at different distances from the spark source.

r_1 (cm)	10	15	20	40	60	100
$\Delta p_+/p_+$ (%)	1	1.5	1.1	0.7	0.5	0.2
$\Delta p_-/p_-$ (%)	6	3	2.6	1.8	1.4	1.2
$\Delta T/T$ (%)	1.2	0.7	0.4	0.2	0.1	0.3
Δt_{ar} (μs)	0.03	0.03	0.03	0.03	0.03	0.03

significantly change. However, choosing the t_s to place the front shock at $r = r_1$ produced more error on the negative peak pressure and minimized the error of the positive peak pressure, and vice versa when the t_s was chosen to place the rear shock at $r = r_1$. Thus, to balance the reconstruction error between the front and the rear shocks, the time shift t_s was chosen to consider the zero crossing point at $r = r_1$.

Thus, despite the validity of the reconstruction algorithm is not demonstrated from a mathematical point of view, the performance and the accuracy of the method is justified.

III. EXPERIMENTAL RESULTS

Measurements were performed at different distances between the spark source and the probing laser beam: 10, 15, 20, 25, 30, 40, 50, 60, 70, 80, and 100 cm. At each distance, 140 waveforms were recorded in order to allow statistical analysis of the data. In the following discussion the distance r_1 is denoted simply as r .

An example of the reconstructed waveform (solid line) with corresponding measured optical phase signal (dashed line) at the distance $r = 20$ cm are presented in Fig. 4. Here, the phase signal is a result of post-processing: low-frequency and high-frequency noise filtering, background phase correction (subtraction of a constant phase level which is present in the signal before arrival of the N -wave), application of a time window to remove reflected waveforms arriving after the direct wave. The order of the magnitude of the optical phase signal is in agreement with Eq. (12): an N -wave with 1250 Pa positive peak pressure resulted in a maximum phase shift of 1 radian.

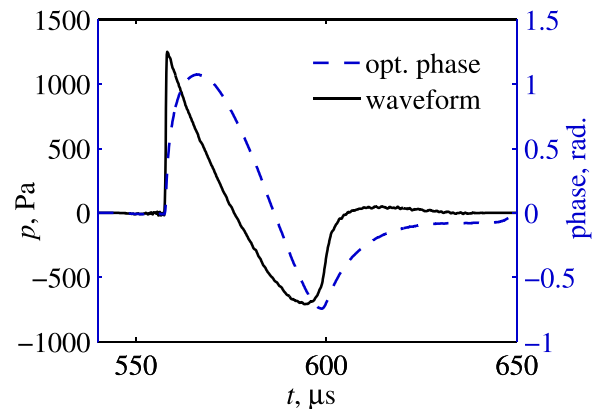


FIG. 4. (Color online) An example of measured waveform at the distance $r = 20$ cm (solid line) and corresponding optical phase signal (dashed line).

Waveforms at several different distances r are shown in Fig. 5. At each distance r , an experimental waveform (solid line) was obtained by averaging 140 individual waveforms, appropriately shifted in time to fit an average arrival time. As expected, close to the source the acoustic wave rather resembles a blast wave than a symmetric N -wave. An experimental waveform at $r = 10$ cm was set as an initial waveform for the Burgers equation (16) to perform numerical simulations, whose results were used to validate measurements. Atmospheric conditions measured during the experiment were $p_0 = 98\,565$ Pa, humidity 40%, temperature 17.6°C . Corresponding air properties were $c_0 = 342.5$ m/s, $\rho_0 = 1.17$ kg/m³, $\gamma = 1.402$, $\beta = 1.20$, $b = 4.5 \times 10^{-5}$ Pa s. The parameters c_ν and τ_ν of relaxation processes were calculated using empirical expressions $c_1 = 0.12$ m/s, $\tau_1 = 6.3$ μs (O₂), $c_2 = 0.022$ m/s, $\tau_2 = 560$ μs (N₂).³¹ The simulated waveforms are shown in Fig. 5 by black dashed lines. An excellent agreement between the experimental and theoretical waveforms is observed, which confirms the measurement method.

Measured and modeled propagation curves of (a) the peak positive (p_+) and peak negative (p_-) pressure, (b) the duration of the compression phase of the waveform (also called half-duration^{5,13}), and (c) the shock rise time τ_{sh} are compared in Figs. 6(a)–6(c). The error bars in Fig. 6 are obtained from statistical processing of 140 measured waveforms. The experimental and theoretical values of the positive peak pressure match to within an interval of 8% (maximal relative difference is noted); negative peak pressure values to within 10%. Application of the technique of least squares to fit the peak positive pressure decrease with a power law function $p_+(r) = p_+(r_0)(r/r_0)^{-\alpha}$ gave an estimation value $\alpha = 1.2$. This exponent value is in good agreement with the exponent reported in Ref. 7, but is different than the values measured in Refs. 36 and 3. This difference may be the result of different propagation distance ranges considered in the cited research papers: $\alpha = 1.27$ in the range from 30 cm to 5 m in Ref. 36 and $\alpha = 1.38$ in the range from 2 to 30 m in Ref. 3.

Half-duration data are also in good agreement within an interval of 2% [Fig. 6(b)]. The increase of the half-duration

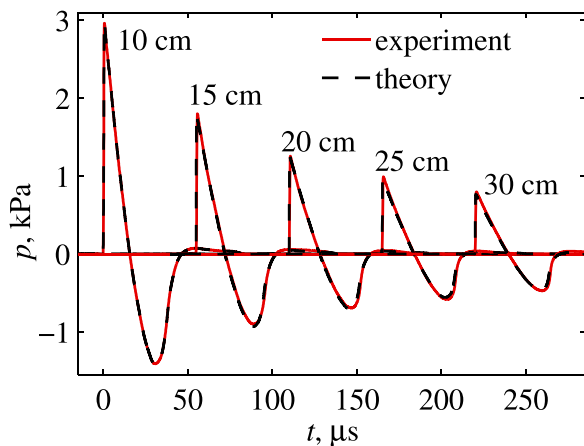


FIG. 5. (Color online) Measured and simulated waveforms at the propagation distances 10, 15, 20, 25, and 30 cm.

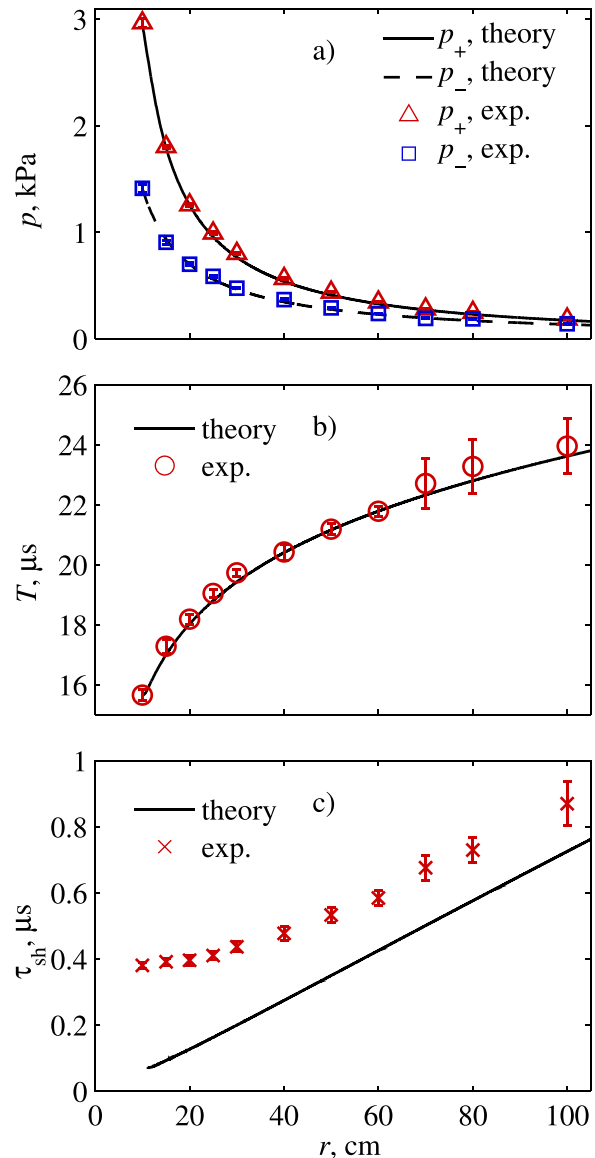


FIG. 6. (Color online) (a) Theoretical (solid line) and experimental (markers) data for the peak positive and peak negative pressures, (b) the half-duration, and (c) the shock rise time.

for larger propagation distances is a classical nonlinear effect.²⁸ Since this effect is amplitude-dependent, it was used to deduce the amplitude of the N -wave.^{5,10,13,20,36} However, with this method it is difficult to achieve an accuracy better than 10%.¹³

Experimental results for the shock rise time are less consistent with theory [Fig. 6(c)]. The rise time is defined as the time for the pressure on the front shock to increase from $0.1 p_+$ to $0.9 p_+$. Experimental values of the rise time are always higher than theoretical values. With the experimental conditions in this work, the time resolution is mainly determined by the laser beam width and focal distance of the focusing lens.³² It follows from Fig. 6(c) that the experimental value of the time resolution is about 0.4 μs . This value is more than 6 times better than that of standard condenser microphones (2.5 – 2.9 μs in the case of the B&K, type 4138) and corresponds to 2.5 MHz bandwidth. Using a better quality laser beam, thinner time resolution can be achieved.

TABLE III. Measured values of the peak positive and peak negative pressures, the half-duration, and the shock rise time from Fig. 6.

r (cm)	10	15	20	25	30	40	50	60	100
p_+ (kPa)	2.97	1.80	1.26	0.99	0.80	0.57	0.438	0.346	0.186
p_- (kPa)	1.41	0.91	0.70	0.59	0.48	0.37	0.292	0.239	0.141
T (μ s)	15.7	17.3	18.2	19.0	19.7	20.4	21.2	21.8	24.0
τ_{sh} (μ s)	0.38	0.39	0.40	0.41	0.44	0.48	0.53	0.58	0.87

However, in the case of strong shocks (tens of kPa or more) or very thin laser beams, diffraction of the optical field on the shock front can lead to degradation of performance of the measurement method.³⁷ For reference, the measured values of the peak positive and peak negative pressures, half-duration, and shock rise time are listed in Table III.

IV. CALIBRATION OF CONDENSER MICROPHONES

Since optical measurements give a more accurate estimation of the pressure wave than microphone measurements, this method was used as a reference to calibrate the microphone. For this purpose, a condenser microphone (B&K, type 4138) was placed 51.2 mm behind the probing beam. Thus, the same propagating acoustic pulse was measured first by the interferometer and then by the microphone (Fig. 1). To account for the difference between positions of the probing laser beam and the microphone, the Burgers equation (16) was used. The optically measured waveform was set as an initial wave, which was propagated forward to the position of the microphone. The simulated optical waveform is shown in Fig. 7(a) by the solid line (in Pa). Microphone

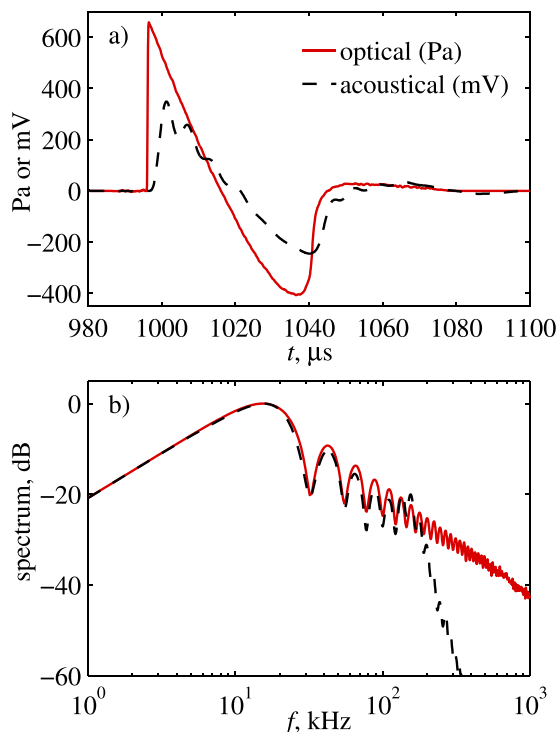


FIG. 7. (Color online) (a) Comparison of a waveform measured using B&K, type 4138 condenser microphone (dashed line) with a waveform obtained by the optical method (solid line) at $r = 30$ cm and propagated 51.2 mm forward. (b) Spectra of the corresponding waveforms.

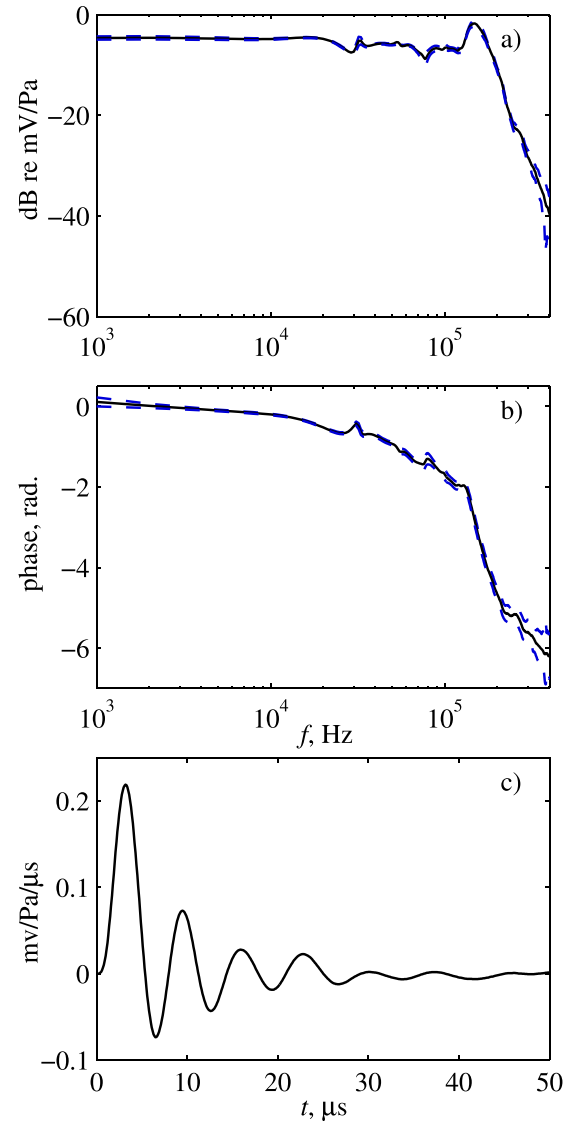


FIG. 8. (Color online) (a) The amplitude of the frequency response of the B&K, type 4138 microphone (solid lines) with ± 3 standard deviation error curves (dashed lines). (b) Phase of the frequency response with ± 3 standard deviation error curves (dashed lines). (c) The impulse response function.

voltage output (in mV) is shown by the black dashed line in the same axes. Resonant response of the condenser microphone is the main cause of oscillations in the voltage waveform. The spectra of the optical and acoustic waveforms, which are normalized at their maxima, are shown in Fig. 7(b). The two spectra are similar at low frequencies, but at high frequencies the spectrum of the acoustic signal exhibits a bandwidth cutoff starting from about 150 kHz. The bandwidth cutoff is explained by the frequency of the mechanical resonance of the microphone membrane and by the frequency response of the amplifier.

The ratio between the spectra of the acoustical and optical signals yields an estimation of the frequency response function of the microphone. The resulting response function was obtained by averaging 140 individual response functions corresponding to waveforms measured under the same conditions. Magnitude (dB relative to 1 mV/Pa) and phase (radians) of the average response function are shown in Figs. 8(a)

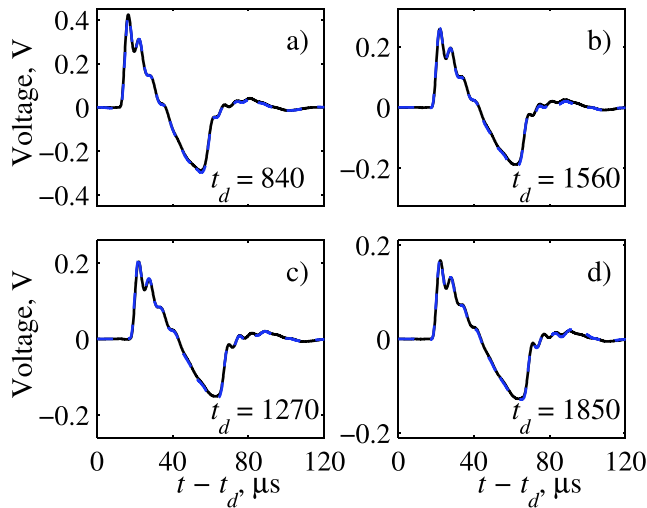


FIG. 9. (Color online) Comparison of waveforms measured using the B&K, type 4138 condenser microphone (solid lines) with waveforms obtained by optical method and filtered by the microphone response (dashed lines) at several distances from the source: (a) $r = 25$, (b) 40, (c) 50, and (d) 60 cm.

and 8(b), respectively. The frequency resolution of the curves in Fig. 8 is 1 kHz. Standard deviation $\sigma(f)$ of the magnitude and phase curves were evaluated at each frequency, and $\pm 3\sigma(f)$ curves are shown in Fig. 8 with dashed lines. The magnitude response has a flat region from the lowest frequencies up to 20 kHz standing at 0.58 mV/Pa level. Between 20 and 80 kHz, irregularities of different amplitudes (1–3 dB) are observed. The resonance peak of +3 dB high above the low-frequency level and of 50 kHz width is centered at 150 kHz. At frequencies higher than the resonant frequency, the response rolls off at approximately -30 dB per octave. Similar structure of the magnitude response is found in the manufacturer's datasheets.¹⁵

The phase curve is almost flat at low frequencies (up to 20 kHz), and then it decreases and jumps around the resonance frequency as expected. The impulse response function obtained by computing the inverse Fourier transform of the frequency response is shown in Fig. 8(c). Oscillations with $7\ \mu\text{s}$ period, which corresponds to the resonance frequency, are clearly seen.

The frequency response function was evaluated using waveforms measured at several other distances r (25, 40, 50, and 60 cm) and similar results were obtained. Optically measured waveforms at these distances were filtered by the frequency response resulting from $r = 30$ cm data (Fig. 9, dashed lines) and compared with corresponding acoustically measured waveforms (Fig. 9, solid lines). An excellent agreement is observed between the acoustical and filtered waveforms, thus validating the proposed calibration method.

The frequency response function was also used to perform deconvolution of acoustic waveforms. Examination of the spectra of these waveforms revealed that after 400 kHz, the spectra amplitude is masked by noise. So, the operation of simple division of the spectra of the acoustical waveforms by the frequency response leads to great amplification of that noise. A Butterworth filter of the fourth order with a cut-off frequency at 400 kHz was applied to reduce the high frequency noise. Results of the acoustic waveform deconvolution are shown in Fig. 10 (dashed lines) for the same distances r as

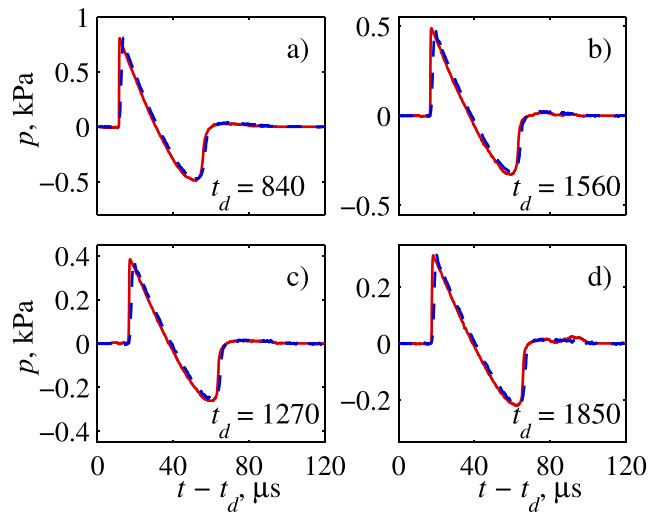


FIG. 10. (Color online) Comparison of waveforms measured using the Mach-Zehnder interferometer (solid lines) with waveforms obtained by deconvolution of the waveforms measured using the B&K, type 4138 condenser microphone with the frequency response from Fig. 8 (dashed lines) at the same distances as in Fig. 9.

in Fig. 9. The deconvolved waveforms are compared with corresponding optically measured waveforms (solid lines). It can be seen that deconvolution allows one to reduce ringing at the resonance frequency of the microphone and to reproduce waveforms which are close to the results of accurate optical measurement except the shock front rise time. The deconvolved waveforms have rise times of about $2\ \mu\text{s}$, while in the optical measurements, it is in the range between 0.4 and $1.0\ \mu\text{s}$, depending on the propagation distance r [Fig. 6(c)].

V. SUMMARY AND CONCLUSIONS

Measurements of spherically diverging nonlinear N -waves in homogenous air were performed using a Mach-Zehnder interferometer. An experimental setup was presented and formation of optical phase signals produced by traveling acoustic waves was explained. The acoustic waveform reconstruction method was proposed and validated in synthetic tests. The method is based on an Abel-type inversion. Tests were conducted by simulating the propagation of acoustic pulses using the generalized Burgers equation. The simulated waveforms were used to form synthetic optical signals. The proposed reconstruction method was applied to simulated optical signals and resulting acoustical waveforms were compared with original ones. The difference between the waveforms with respect to amplitude and to half-duration was about 2% or less.

Measurements were performed for several propagation distances in a range from 10 to 100 cm. An experimental waveform at $r = 10$ cm was used to set boundary conditions for the generalized Burgers equation and a numerical simulation was run up to $r = 100$ cm. Measured waveforms were compared with simulated waveforms and excellent agreement was demonstrated at all distances. Analysis of the shock rise time has shown that the interferometric method allows one to reach a time resolution of $0.4\ \mu\text{s}$, which is more than 6 times better than the time resolution of standard condenser microphones (2.5 – $2.9\ \mu\text{s}$ in the case of B&K, type 4138).

Optical measurements have been used to calibrate an acoustical microphone (B&K, type 4138). The microphone was placed 51.2 mm behind the probing laser beam. Thus, the same acoustic wave was measured by the optical method and by the microphone. Numerical simulations with the Burgers equation were used to account for the propagation distance difference between the laser beam and the microphone. The frequency response of the microphone was obtained by dividing the spectra of the optical and acoustical waveforms. It was shown that at different available propagation distances, the optically measured waveforms filtered with the frequency response are in good agreement with the waveforms measured by the acoustical microphone.

Thus, the optical measurement method based on a Mach-Zehnder interferometer provided accurate characterization of high amplitude shock pulses in laboratory experiments in air and permitted the definition of a new calibration method for broadband condenser microphones.

ACKNOWLEDGMENTS

This work was supported by ANR Program 2010, Grant No. BLAN 0905 03 (SIMMIC), the French/Russian Program for International Scientific Cooperation, Grant No. PICS RFBR 10-02-91062 /CNRS 5603, by the grant of the President of Russia, Grant No. MK-5895.2013.2, and by the RFBR Grant No. 12-02-31830-mola. This work was conducted in the framework of the LabEx CeLyA (“Centre Lyonnais d’Acoustique,” Grant No. ANR-10-LABX-60). The authors would like to thank Jean-Michel Perrin for his help in setting up the experiment. The authors are also grateful to Emmanuel Jondeau for his help during installation of the acquisition system, to Loic Mèès for helpful discussions on optics adjustment, to Frédéric Ferrand for fabrication of electronic devices, and to Olivier Marsden for the helpful comments on the manuscript.

APPENDIX: STABILIZATION SYSTEM FUNCTIONING

The stabilization system allows one to keep the optical phase of the Mach-Zehnder interferometer at a certain fixed value despite the different low-frequency mechanical and acoustical perturbations of the optical path (noise, vibrations).

The stabilization system uses a feedback principle. As was described in Sec. II A 2, the signal of the second output of the differential amplifier [$u_{fb}(t) = -u(t)$, where the signal $u(t)$ is given by Eq. (4)] was filtered with a low-pass filter and was connected to an input of a low-frequency amplifier, which drives the piezoactuator. Thus, the voltage on the piezoactuator is given as a convolution,

$$u_{pz}(t) = \int_{-\infty}^t H(t-t')u_{fb}(t')dt'. \quad (\text{A1})$$

Here, $H(t)$ is a combined impulse response function characterizing the low-pass filter and the amplifier of the piezoactuator. Since the fraction of the optical phase which is controlled by the piezodriver is proportional to the voltage u_{pz} [Eq. (1)], the following equation is valid:

$$\begin{aligned} \varphi_{pz}(t) = & -\alpha \int_{-\infty}^t H(t-t') \\ & \times u_0 \cos(\varphi_0 + \varphi_{pz}(t') + \varphi_{ac}(t') + \varphi_n(t'))dt'. \end{aligned} \quad (\text{A2})$$

This is a nonlinear integral equation for the function $\varphi_{pz}(t)$ if the signals $\varphi_{ac}(t)$ and $\varphi_n(t)$ are given. For the sake of simplicity, consider a low-pass filter, which corresponds to an integrating circuit. The amplifier of the piezodriver is characterized by a constant gain h , since its cut-off frequency is about several tens of kHz (see Sec. II), while the low pass filter is supposed to have its cut-off frequency at several hundreds of Hz. Thus, Eq. (A2) can be rewritten as

$$\varphi_{pz}(t) = -\frac{\alpha h}{T_i} \int_{-\infty}^t u_0 \cos(\varphi_0 + \varphi_{pz}(t') + \varphi_{ac}(t') + \varphi_n(t'))dt'. \quad (\text{A3})$$

Here, T_i is the time constant of the integrating circuit. Differentiation of Eq. (A3) with respect to time gives

$$\frac{\partial \varphi_{pz}(t)}{\partial t} = -\frac{\alpha h}{T_i} u_0 \cos(\varphi_0 + \varphi_{pz}(t) + \varphi_{ac}(t) + \varphi_n(t)). \quad (\text{A4})$$

If the acoustical phase φ_{ac} and the noise phase φ_n are equal to zero, the piezoactuator moves the optical phase difference to an equilibrium state, which is defined by the condition

$$\frac{\partial \varphi_{pz}(t)}{\partial t} = 0 \quad \text{or} \quad \cos(\varphi_0 + \varphi_{pz0}) = 0. \quad (\text{A5})$$

Thus, phase values at equilibrium states are $\varphi_0 + \varphi_{pz0} = -\pi/2 + 2\pi m$, where m is an integer number. In the neighborhood of an equilibrium point the feedback equation can be represented as

$$\frac{\partial \tilde{\varphi}_{pz}(t)}{\partial t} = -\frac{\alpha h u_0}{T_i} \sin(\tilde{\varphi}_{pz}(t) + \varphi_{ac}(t) + \varphi_n(t)). \quad (\text{A6})$$

Here, $\tilde{\varphi}_{pz}(t) = \varphi_{pz}(t) - \varphi_{pz0}$ is the difference between time-variant phase shift of the piezoactuator and the constant equilibrium phase. In this case, the measured optical signal [Eq. (4)] is expressed as

$$u = u_0 \sin(\tilde{\varphi}_{pz}(t) + \varphi_{ac}(t) + \varphi_n(t)). \quad (\text{A7})$$

The differential equation (A6) can be analyzed analytically if all phases are small ($\tilde{\varphi}_{pz}(t), \varphi_{ac}(t), \varphi_n(t) \ll 1$) and thus, the equation can be linearized,

$$\frac{\partial \tilde{\varphi}_{pz}(t)}{\partial t} = -\beta(\tilde{\varphi}_{pz}(t) + \varphi_{ac}(t) + \varphi_n(t)), \quad (\text{A8})$$

where a constant $\beta = \alpha h u_0 / T_i$ is introduced. The measured optical signal [Eq. (A7)] transforms to

$$u = u_0(\tilde{\varphi}_{pz}(t) + \varphi_{ac}(t) + \varphi_n(t)). \quad (\text{A9})$$

In the frequency domain the solution of the linearized feedback Eq. (A8) is

$$\hat{\varphi}_{pz}(\omega) = \frac{-\beta}{i\omega + \beta} (\hat{\varphi}_{ac}(\omega) + \hat{\varphi}_n(\omega)). \quad (\text{A10})$$

Here $\hat{\varphi}_{pz}(\omega)$, $\hat{\varphi}_{ac}(\omega)$, and $\hat{\varphi}_n(\omega)$ are the Fourier spectra of the signals $\tilde{\varphi}_{pz}(t)$, $\varphi_{ac}(t)$, and $\varphi_n(t)$, respectively. Substitution of the solution (A10) in the frequency domain version of Eq. (A9) produces

$$\hat{u}(\omega) = u_0 \frac{i\omega}{i\omega + \beta} (\hat{\varphi}_{ac}(\omega) + \hat{\varphi}_n(\omega)). \quad (\text{A11})$$

It can be seen from Eq. (A11), that the sum of the acoustic wave phase signal and the noise is filtered with a high-pass filter with characteristic frequency $\beta/2\pi$ Hz. If characteristic frequencies of the noise are lower than $\beta/2\pi$ and characteristic signal frequencies are higher than $\beta/2\pi$, then the noise is effectively removed. The frequency $\beta/2\pi$ in the given experimental conditions was equal to about 100 Hz.

If an arbitrary frequency response of the filter is considered $[\hat{H}(\omega)]$, then the solution of the same linearized problem is

$$\hat{\varphi}_{pz}(\omega) = -\frac{\alpha u_0 h \hat{H}(\omega)}{i\omega + \alpha u_0 h \hat{H}(\omega)} (\hat{\varphi}_{ac}(\omega) + \hat{\varphi}_n(\omega)), \quad (\text{A12})$$

$$\hat{u}(\omega) = u_0 \frac{i\omega}{i\omega + \alpha u_0 h \hat{H}(\omega)} (\hat{\varphi}_{ac}(\omega) + \hat{\varphi}_n(\omega)). \quad (\text{A13})$$

- ¹J. DuMond, E. Cohen, W. Panofsky, and E. Deeds, "A determination of the wave forms and laws of propagation and dissipation of ballistic shock waves," *J. Acoust. Soc. Am.* **18**, 97–118 (1946).
- ²A. Loubeau, V. Sparrow, L. Pater, and W. Wright, "High-frequency measurements of blast wave propagation," *J. Acoust. Soc. Am.* **120**, EL29–EL35 (2006).
- ³H. Honma, I. Glass, C. Wong, O. Holst-Jensen, and D. Xu, "Experimental and numerical studies of weak blast waves in air," *Shock Waves* **1**, 111–119 (1991).
- ⁴Q. Qin and K. Attenborough, "Characteristics and application of laser-generated acoustic shock waves in air," *Appl. Acoust.* **65**, 325–340 (2004).
- ⁵W. Wright, "Propagation in air of N -waves produced by sparks," *J. Acoust. Soc. Am.* **73**, 1948–1955 (1983).
- ⁶M. Hargather and G. Settles, "Optical measurement and scaling of blasts from gram-range explosive charges," *Shock Waves* **17**, 215–223 (2007).
- ⁷J. Reed, "Atmospheric attenuation of explosion waves," *J. Acoust. Soc. Am.* **61**, 39–47 (1977).
- ⁸J. Picaut, T. L. Pollès, P. L'Hermite, and V. Gary, "Experimental study of sound propagation in a street," *Appl. Acoust.* **66**, 149–173 (2005).
- ⁹J. Gómez Bolaños, V. Pulkki, P. Karppinen, and E. Hægström, "An opto-acoustic point source for acoustic scale model measurements," *J. Acoust. Soc. Am.* **133**, EL221–EL227 (2013).
- ¹⁰B. Lipkens and D. Blackstock, "Model experiment to study sonic boom propagation through turbulence. Part I: Model experiment and general results," *J. Acoust. Soc. Am.* **103**, 148–158 (1998).
- ¹¹S. Ollivier and P. Blanc-Benon, "Model experiment to study acoustic N -wave propagation through turbulence," in *Proceedings of the 10th AIAA/CEAS Aeroacoustics Conference*, AIAA2004-2921, Manchester, United Kingdom (2004).
- ¹²M. Averiyarov, S. Ollivier, V. Khokhlova, and P. Blanc-Benon, "Random focusing of nonlinear acoustic N -waves in fully developed turbulence: Laboratory scale experiment," *J. Acoust. Soc. Am.* **130**, 3595–3607 (2011).
- ¹³P. Yuldashev, S. Ollivier, M. Averiyarov, O. Sapozhnikov, V. Khokhlova, and P. Blanc-Benon, "Nonlinear propagation of spark-generated N -waves in air: Modeling and measurements using acoustical and optical methods," *J. Acoust. Soc. Am.* **128**, 3321–3333 (2010).
- ¹⁴G.R.A.S., "Measurement microphone sets," URL <http://www.gras.dk/products/measurement-microphone-sets.html> (Last viewed June 30, 2014).
- ¹⁵B&K, "Microphones," URL <http://www.bksv.com/Products/transducers/acoustic/microphones/microphone-cartridges> (Last viewed June 30, 2014).
- ¹⁶W. Wright and J. McKittrick, "Diffraction of spark-produced acoustic impulses," *Am. J. Phys.* **35**, 124–128 (1967).
- ¹⁷S. Horowitz, T. Nishida, L. Cattafesta, and M. Sheplak, "Development of a micromachined piezoelectric microphone for aeroacoustics applications," *J. Acoust. Soc. Am.* **122**, 3428–3436 (2007).
- ¹⁸Z. Zhou, L. Rufer, E. Salze, P. Yuldashev, S. Ollivier, and M. Wong, "Bulk micromachined wide-band aero-acoustic microphone and its application to acoustic ranging," *J. Micromech. Microeng.* **23**, 105006 (2013).
- ¹⁹M. Kuntzman and N. Hall, "A broadband, capacitive, surface-micromachined, omnidirectional microphone with more than 200 kHz bandwidth," *J. Acoust. Soc. Am.* **135**, 3416–3424 (2014).
- ²⁰P. Yuldashev, M. Aver'yanov, V. Khokhlova, S. Ollivier, and P. Blanc-Benon, "Nonlinear spherically divergent shock waves propagating in a relaxing medium," *Acoust. Phys.* **54**, 32–41 (2008).
- ²¹G. S. Settles, *Schlieren and Shadowgraph Techniques: Visualizing Phenomena in Transparent Media*, 1st ed. (Springer-Verlag, Heidelberg, 2001), Chap. 2, pp. 25–37.
- ²²W. Merzkirch, *Flow Visualization* (Academic, New York, 1974), pp. 62–102.
- ²³T. Mizukaki, "Application of digital phase-shift holographic interferometry to weak shock waves propagating at mach 1.007," *Shock Waves* **20**, 19–27 (2010).
- ²⁴A. Torras-Rosel and S. Barrera-Figueroa, "Sound field reconstruction using acousto-optic tomography," *J. Acoust. Soc. Am.* **131**, 3786–3793 (2012).
- ²⁵K. Nakamura, "Sound field measurement through the acousto-optic effect of air by using laser Doppler velocimeter," in *Proceedings of the 4th Pacific Rim Conference on Lasers and Electro-Optics, 2001. CLEO/Pacific Rim 2001* (2001), Vol. 1, p. I–154.
- ²⁶N. Bilaniuk, "Optical microphone transduction techniques," *Appl. Acoust.* **50**, 35–63 (1997).
- ²⁷G. Smeets, "Laser interference microphone for ultrasonics and nonlinear acoustics," *J. Acoust. Soc. Am.* **61**, 872–875 (1977).
- ²⁸O. V. Rudenko and S. I. Soluyan, *Theoretical Foundations of Nonlinear Acoustics* (Consultants Bureau, New York, 1977).
- ²⁹J. Graeme, *Photodiode Amplifiers: OP AMP Solutions*, 1st ed. (McGraw-Hill, New York, 1996), Chaps. 1–4.
- ³⁰M. Born and E. Wolf, *Principles of Optics*, 7th ed. (Cambridge University Press, Cambridge, 1999), Chap. VII, pp. 286–290.
- ³¹A. D. Pierce, *Acoustics: An Introduction to its Physical Principles and Applications* (McGraw-Hill, New York, 1981), pp. 11–28, 553–555.
- ³²P. Yuldashev, M. Averiyarov, V. Khokhlova, O. Sapozhnikov, S. Ollivier, and P. Blanc-Benon, "Measurement of shock N -waves using optical methods," in *Proceedings of the 10th French Acoustical Conference*, Lyon, 12–16 April 2010.
- ³³R. N. Bracewell, *The Fourier Transform and Its Applications*, 3rd ed. (McGraw-Hill, New York, 2000), pp. 351–356.
- ³⁴E. Lemmon, R. Jacobsen, S. Penoncello, and D. Friend, "Thermodynamic properties of air and mixtures of nitrogen, argon and oxygen from 60 to 2000 K at pressures to 2000 MPa," *J. Phys. Chem. Ref. Data* **29**, 331–385 (2000).
- ³⁵M. Jarraud *et al.*, *Guide to Meteorological Instruments and Methods of Observation*, 7th ed. (World Meteorological Organization, Geneva, Switzerland, 2008), pp. I. 4-26–I. 4-29.
- ³⁶L. Orenstein, "The rise time of N -waves produced by sparks," Technical Report No. ARL-TR-82-51, Applied Research Laboratories, University of Texas–Austin (1982).
- ³⁷J. Panda and G. Adamovsky, "Laser light scattering by shock waves," *Phys. Fluids* **7**, 2271–2279 (1995).